An online fault-diagnosis of electromagnetic actuator based on variation characteristics of load current

Xin Cheng, Baixin Cheng, Meiqian Lu, Rougang Zhou & Lin Zhang

Published online: 07 Nov 2019.

Submit your article to this journal ⬚

Article views: 274

View related articles ⬚

View Crossmark data ⬚

Citing articles: 1 View citing articles ⬚

Taylor & Francis
Taylor & Francis Group

An online fault-diagnosis of electromagnetic actuator based on variation characteristics of load current

Xin Cheng[a,b], Baixin Cheng[a], Meiqian Lu[a], Rougang Zhou[c] and Lin Zhang[a]

[a] School of Mechanical & Electronic Engineering, Wuhan University of Technology, Wuhan, People's Republic of China; [b] Hubei Maglev Engineering Technology Research Center, Wuhan University of Technology, Wuhan, People's Republic of China; [c] School of Mechanical Engineering, Hangzhou Dianzi University, Hangzhou, People's Republic of China

ABSTRACT

Accurate and fast fault-diagnosis is the foundation of fault-tolerance. To develop the fault-tolerance of magnetic-levitated bearing system, this paper presents an online fault-diagnosis approach of electromagnetic actuator based on variation characteristics of sampled load current in the modulation to identify the time constant of the electromagnetic coil, and then to diagnose the broken circuit or partial short-circuit faults. After analysing the variation characteristics of the load current theoretically, the simulation is constructed to verify the effectiveness of the proposed approach. Considering the real-time requirement of fault-diagnosis, we develop a fast sampling and calculating method for the equivalent slope of the load current in the modulation, which represents the variation characteristics of the load current. The experimental results demonstrate that the proposed approach is effective for diagnosing broken circuit and partial short-circuit faults, and the execution time for the fault-diagnosis is about 2 ms, proving its excellent real-time performance.

1. Introduction

Magnetic-levitated actuator, with the advantages of no mechanical friction, no lubrication and controllable supporting characteristics [1,2], has two forms of plane and rotary motion mainly. MLPAs (magnetically levitated planar actuators) [1,3–6], which belong to the former category, are mainly used in the ultra-precision multi-DOF (degree of freedom) stage [7]. Magnetic-levitated bearings, belonging to the latter, are the key equipment in the aero engine, turbine generator, energy storage flywheel, etc. [8,9].

To the rolling bearing or gear, the most common mechanical components in rotating machines, numerous vibration-based fault-diagnosis or health indicators [10] have been constructed from mechanical signal processing [11,12], modelling [13,14], or stochastic process [15], and provides a basis for predicting the remaining useful life of bearings and gears. However, magnetic-levitated bearing system is a highly nonlinear and open-loop unstable system, the rotor is supported by controlled EMF (electromagnetic forces) generated by symmetrical electromagnetic actuators. The basic control theory is based on the bias current linearization in the equilibrium position, namely, displacement-force and current-force stiffness coefficient are used to realize the linearization of EMF [2], which has the symmetry constraints on the stator structure. Therefore,

the actuator failure is one of the most common faults, and it will destroy the original symmetry of the stator structure, resulting in the control failures of related free degree. As a result, the rotor will fall, leading to the serious damages to the whole bearing system [16]. Therefore, it is difficult to adopt health indicators to estimate the lifetime of the magnetic-levitated bearing system.

Design of the redundant actuators is an effective means to deal with the failures in the magnetic-levitated bearing system, but accurate and fast fault-diagnosis of electromagnetic actuators is the crucial foundation. However, the controlled currents for the electromagnetic actuators are usually provided by PA (Power amplifier); moreover, a close-loop control of current is designed, including the current sensor, controller, and electromagnetic coil. The fault of any one will cause the failure of the corresponding electromagnetic actuator. The common forms of faults include the broken circuits, short circuits and the partial insulation damage of the electromagnetic coil, leading to the deviation of the EMF model [17], or even the damage to the bearing system.

The fault detection and diagnosis of electromagnetic actuators can be mainly categorized into the following approaches. The first one is based on the mathematical model to analyse different faults, but it is difficult to

CONTACT Rougang Zhou ✉ zhourg@hdu.edu.cn 🖂 School of Mechanical Engineering, Hangzhou Dianzi University, Hangzhou 310000, People's Republic of China

establish sufficiently accurate models of various faults at various operations [18]. The second approach uses signal processing-based methods. The currents and vibration signals can be obtained most easily and they have been used for the detection of stator, rotor and bearing faults [19, 20]. Machine current signature analysis (MCSA) is a popular approach used in fault-diagnosis of induction motor, which monitors current in time and frequency-domain characteristics, from healthy to faulty condition, can detect faults by using only current sensors [21]. However, this method fails to detect broken faults under a no-load condition because load current is comparatively small, not available enough for fault analysis. To overcome this problem, discrete wavelet analysis and higher order spectra were proposed in an unloaded condition [22,23]. In addition, a modified bispectrum based on the amplitude modulation feature of the current signal was then adopted in [24] to combine both lower sidebands and higher sidebands simultaneously, and an effective diagnostic feature was developed for fault classification based on this new bispectrum analysis. A fault detection approach based on GLRT (Gaussian generalized likelihood ratio test) was proposed in [25] to detect the faults in the electromagnet, and the accuracy of this approach had been proved by numerical analysis, however, usually the effective thresholds from experiences were needed in this approach; while in [26], the Hilbert transform was used to process the current signal and extract a signature related to a broken rotor bar fault under a no-load condition, but its actual effectiveness needs to be proved. Moreover, some intelligent approaches for fault-diagnosis in a single-input, single-output active magnetic bearing system was developed and experimentally demonstrated in [27] by using an augmented linear model of the plant dynamics together with a Kalman filter to estimate fault states; and in [28] by using state estimator and parameter estimator to detect, identify and analyse faults of actuators in magnetic-levitated bearing system. A fuzzy decision tree was designed to detect broken rotor bars and broken connector faults by the measuring of one phase current signal to construct the phase space representation [29]. A robust adaptive sliding mode thau observer is proposed to estimate the time-varying magnitudes of actuator faults based on the dynamics of the quadcopter in [30,31], and then a fault-tolerant control scheme based on sliding mode control and reconfiguration technique is designed in [31]. Glowacz [32] proposed an acoustic-based fault detection of the commutator motors by using nearest mean (NM) and support vector machine (SVM) classifiers for data classification. Although the efficiency of above approaches has been proved, the relevant algorithms are complex, leading to the real-time performance difficult to satisfy the requirement of high-speed magnetic bearing applications. Freddi et al. [33] investigated a model-based fault-diagnosis which can

be used to monitor sensor faults and detect actuator faults. In this method, residuals are used to distinguish between system and observer outputs, but these methods are inaccurate and unsuitable for quantifying the magnitude of a fault. By using a bank of filters, with thresholds defined in a way that they explicitly account for the effect of uncertainty, a fault detection and isolation (FDI) approach was proposed to the actuator and sensor fault-diagnosis for nonlinear uncertain systems [34]; another simple and useful approach based on threshold was proposed in [35] by monitoring the error between the load current and current set point, but it is also difficult to find the effective thresholds.

A new scheme of reconstructing current sensor faults and estimating unknown load disturbance for a permanent magnet synchronous motor (PMSM)-driven system in [36]. Two sliding mode observers (SMOs) are designed: the unknown load disturbance is estimated by the first SMO in the subsystem, which has unknown load disturbance, and the sensor faults can be reconstructed using the second SMO in the augmented subsystem, which has sensor faults. However, an immediate response should be made by the control system if the failures of some actuators happen, or the drop of the magnetic-levitated rotor will cause the damages to the bearing system. Eric and Meeker [37] proposed the generalized bias current linearization, which can compensate the loss of magnetic flux due to the failures of the actuators by the way of current distribution to achieve the fault-tolerance. Relying on the coupled magnetic circuit between the adjacent magnetic poles, the loss of magnetic flux caused by the failures of some actuators can be compensated by the fault-tolerant controller discussed in [37]. Based on this idea, the subsequent researches [38–42] were developed to reconfigure the support structure.

This paper presents a novel online FDD (fault detection and diagnosis) approach of the electromagnetic actuator based on the variation characteristics of the load current in the modulation to identify the time constant of the electromagnetic coil. With respect to the literature, the proposed approach has the advantages of (1) theoretic thresholds and (2) excellent real-time performance. Experimental results prove the effectiveness and real-time performance of the proposed approach. This novel FDD approach can be combined with the generalized bias current linearization in [37] to realize an effective design of the fault-tolerant controller of magnetic-levitated bearings under the failures of the electromagnetic actuators.

2. Mathematical proof of variation characteristics of load current

The block diagram of digital PA is shown in Figure 1. The desired current of the electromagnetic coil will be produced under the close-loop control. CT_1 and
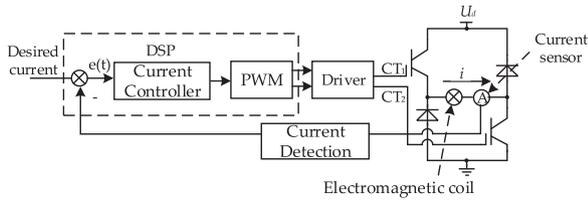
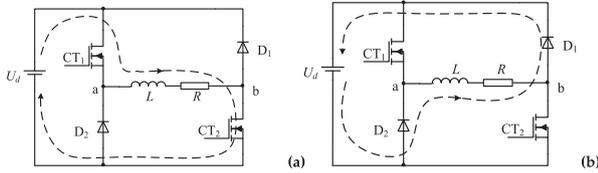**Figure 1.** Block diagram of power amplifier.

Figure 2. Current flows under bi-state modulation, (a) current increasing process, (b) current deceasing process.

CT$_2$, respectively, drive the upper and lower sides of the power bridge, with the duty cycle implied to control the change of the current in the coil. Under the control of current controller (usually PID), the error of current loop will be close to zero, making the load current in coil equalling to the desired one. The current controller can be realized in a DSP (digital signal processor), and the controlled duty cycle can be transferred into PWM signal by the PWM module of DSP. There are two kinds of processes (in bi-state mode) in Figure 2(a,b), respectively.

2.1. Current increasing process

When CT$_1$ and CT$_2$ are enabled synchronously, the load current i in the electromagnetic coil will increase, and the differential equation of the circuit can be expressed as

$$U_d = L\frac{di(t)}{dt} + Ri(t) + 2U_s \qquad (1)$$

where U_d is the bus power supply voltage; U_s is the conduction voltage drop of the switch tube, which is a constant for a certain type of switch tube. L and R are the equivalent inductance and resistance of the coil, respectively. By solving Equation (1), we can have

$$i(t) = \frac{U_d - 2U_s}{R}(1 - e^{-\frac{t}{\tau}}) + i_0 e^{-\frac{t}{\tau}} \qquad (2)$$

k_{inc}, the slope of load current in the increasing process, can be obtained as

$$k_{inc} = \frac{di(t)}{dt} = \frac{U_d - 2U_s}{L}e^{-\frac{t}{\tau}} - \frac{i_0}{\tau}e^{-\frac{t}{\tau}} \qquad (3)$$

We must note that k_{inc} describes the variation characteristics of load current in the modulation, and will change in different phase theoretically. However, $\tau = L/R$, the time constant of the electromagnetic coil,
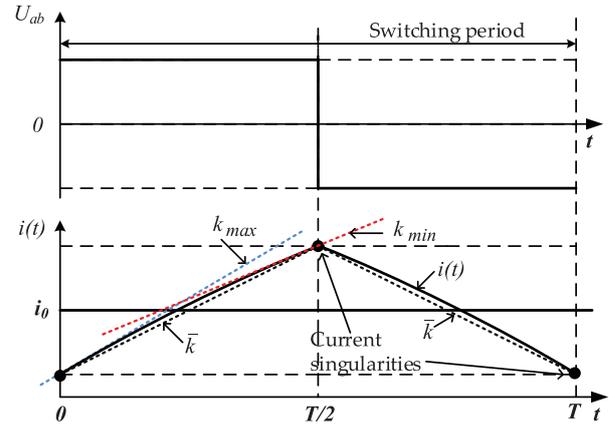

Figure 3. The slopes of the load current in the switching period.

is much larger than switching period T, so Equation (3) can be approximated as

$$k_{inc} = \frac{U_d - 2U_s}{L} - \frac{i_0}{\tau} = \frac{U_d - 2U_s - i_0R}{L} \qquad (4)$$

where i_0 is the initial current of the electromagnetic coil in the switching period.

2.2. Current deceasing process

When CT$_1$ and CT$_2$ are disabled synchronously, the load current will decrease, and the differential equation is as

$$-U_d = L\frac{di(t)}{dt} + Ri(t) + 2U_c \qquad (5)$$

where U_c is the conduction voltage drop of freewheeling diode D_1 or D_2. We can have

$$i(t) = -\frac{U_d + 2U_c}{R}(1 - e^{-\frac{t}{\tau}}) + i_0 e^{-\frac{t}{\tau}} \qquad (6)$$

$$k_{dec} = \frac{di(t)}{dt} = -\frac{U_d + 2U_c}{L}e^{-\frac{t}{\tau}} - \frac{i_0}{\tau}e^{-\frac{t}{\tau}} \qquad (7)$$

Similarly, k_{dec}, the slope of load current in the decreasing process, can be approximated as

$$k_{dec} = -\frac{U_d + 2U_c}{L} - \frac{i_0}{\tau} = -\frac{U_d + 2U_c + i_0R}{L} \qquad (8)$$

Obviously, from Equations (3) and (7), either k_{inc} or k_{dec} will change in different phase theoretically, but they all have the limiting values. Taking k_{inc} as an example, we can have its limiting values in Equation (9) at $t = 0$ or $T/2$, as in Figure 3.

$$k_{\max} = \frac{U_d - 2U_s}{L} - \frac{i_0}{\tau}$$

$$k_{\min} = \frac{U_d - 2U_s}{L} \cdot e^{-\left(\frac{T}{2}\right)/\tau} - \frac{i_0}{\tau} \cdot e^{-\left(\frac{T}{2}\right)/\tau} \qquad (9)$$

Considering the τ (ms level) is much larger than switching period T (us level), we can have

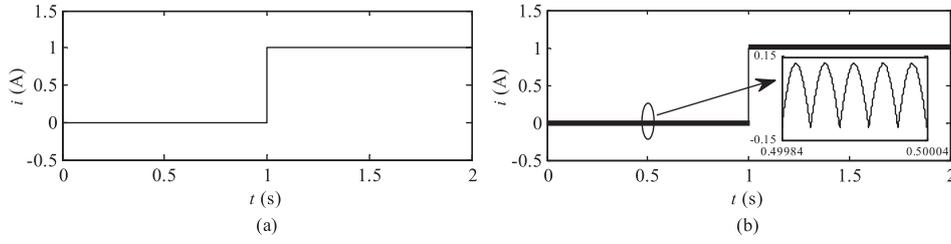$$k_{\min} \approx k_{\max} \approx k_{inc} = \frac{U_d - 2U_s - i_0R}{L} \qquad (10)$$

Figure 4. Simulation results: (a) excitation signal, (b) load current.

From Equation (10), R is coil resistor (usually mΩ level), so $i_0 R$ can be ignored compared with bus voltage U_d in most of the application, which means that the variation characteristics of the load current are the inherent characteristics of the electromagnetic coil in the switching period, and the influence of load current to the slopes can be very small.

In short, k_{inc} and k_{dec} can almost be one constant in the switching period, and decided by the time constant of the electromagnetic coil directly, namely, FDD can be applied by identifying the variation characteristics of load current. Figure 3 illustrates the slopes of the load current in the switching period, the first phase from $t = 0$ to $T/2$ corresponds to the current increasing process in Section 2.1 while another phase $(T/2, T)$ to the current decreasing process in Section 2.2. We define the equivalent slope $\bar{k}$ to approximate the slope of the load current in the each phase, and it will be very close to the average value of k_{inc}.

3. Simulation verification and analysis

From Figure 3, ignoring the U_s and U_c, the load voltage is

$$U_{ab} \approx \begin{cases} +U_d, & nT \le t \le nT + t_1 \\ -U_d, & nT + t_1 \le t \le (n+1)T \end{cases} \quad (11)$$

$$\text{and } t_1 = TU_f/U_t \quad (12)$$

where U_f is the modulated signal input by the PWM generator, U_t is the unilateral amplitude of the triangular carrier, T is the switching period, and nT is the nth switching period. In the $[nT, (n+1)T]$, U_{ab} can be expanded by Fourier series, as

$$U_{ab} = \frac{a_0}{2} + \sum_{k=1}^{\infty} a_k \cos(k\omega t) + \sum_{k=1}^{\infty} b_k \sin(k\omega t) \quad (13)$$

The expressions of a_0, a_k and b_k are as

$$a_0 = \frac{2}{T} \int_{nT}^{(n+1)T} U_{ab} dt = \left(4\frac{U_f}{U_t} - 2 \right) U_d \quad (14)$$

$$a_k = \frac{2}{T} \int_{nT}^{(n+1)T} U_{ab} \cos(k\omega t) dt = \frac{2U_d}{k\pi} \sin\left(2k\pi \frac{U_f}{U_t} \right) \quad (15)$$

$$b_k = \frac{2}{T} \int_{nT}^{(n+1)T} U_{ab} \sin(k\omega t) dt$$

$$= \frac{2U_d}{k\pi} \left[1 - \cos\left(2k\pi \frac{U_f}{U_t} \right) \right] \quad (16)$$

By introducing Equations (14)–(16) into the (17), we can have

$$U_{ab} = \left(2\frac{U_f}{U_t} - 1 \right) U_d$$

$$+ \sum_{k=1}^{\infty} \frac{2U_d}{k\pi} \left[\sin\left(2k\pi \frac{U_f}{U_t} - k\omega t \right) + \sin(k\omega t) \right] \quad (17)$$

$$\frac{i_{ab}}{U_{ab}} = \frac{1}{R + Ls} \quad (18)$$

We establish the simulation model with the switching frequency of 25 kHz, the bus voltage of 30 V, and an electromagnetic coil of 0.5 Ω, 2 mH. By applying a step, amplitude of 1 A excitation signal as the desired current, we have the simulation results in Figure 4. The load current can follow the desired current with its variation characteristics consistent with the theoretical analysis. Selecting another electromagnetic coil of 0.2 Ω, 1 mH, the comparable simulation results are shown in Figure 5, where the slope of current variation changes with different coils.

Generally, the slope of a series of discrete sampling points can be obtained by linear fitting, in order to improve the real-time performance, a more effective and simpler method is designed in this paper through the average of the slopes between every two adjacent sampling points. Setting a_n as the digital value of load
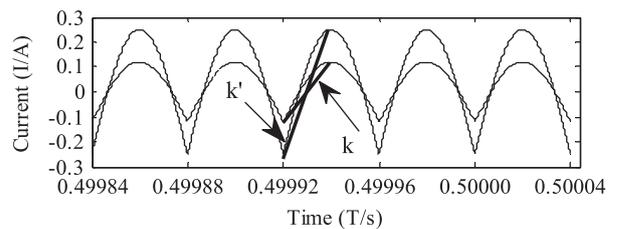

Figure 5. Simulation results under different time constant. The slope of k corresponds to 0.5 Ω, 2 mH coil, while k' corresponds to 0.2 Ω, 1 mH coil.
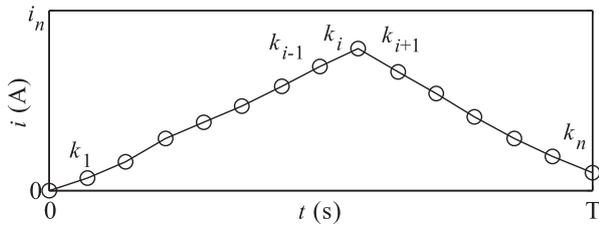
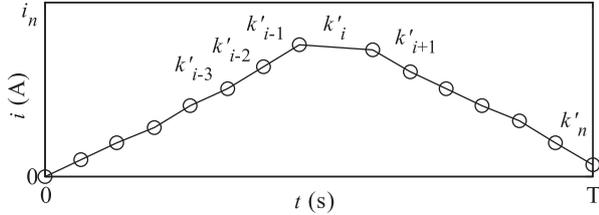**Figure 6.** Slope of current variation between two adjacent sampling points.

Figure 7. Singularity in the sampling points.

current sampled currently, and the next is a_{n+1}, $n = 1$, $2 \ldots$. The slope of two adjacent sampling points can be expressed as

$$k_n = \frac{G_f(a_{n+1} - a_n)U_{ref}}{2^m R_a T_n} \tag{19}$$

where G_f is the attenuation coefficient of the current sensor, R_a is the sampling resistance, T_n, U_{ref} and m are the sampling period, reference voltage and resolution of AD (analogue–digital) converter, respectively. A series of slopes values can be obtained, as shown in Figure 6.

Taking the current increasing process as an example, k_1, k_2, k_{i-1} and k_i are a series of slopes, and the average value can be calculated as

$$\bar{k} = \frac{k_1 + k_2 + \cdots k_{i-1} + k_i}{i} \tag{20}$$

According to the theoretical analysis in Section 2, these slopes, representing the k_{inc} in different time, will change from the k_{min} to k_{max}, and repeat the same process in every switching period. Actually, for the k_{min} and k_{max} are very close in the switching period, the k_i can

almost be a constant like k_{inc}. Therefore, we can adopt the $\bar{k}$ to approximate the slope of the load current in each phase, as in Figure 3, and faults can be detected by comparing $\bar{k}$ with the thresholds in Equation (9) theoretically.

It is important to note that the singularities in the sampling points will be likely an error factor in the calculation of $\bar{k}$. Therefore, it is necessary to make an effective judgment to cancel the singularities. The algorithm is designed by the following rules: (1) k'_i is positive and its two adjacent k'_{i-1} and k'_{i+1} are also positive, or (2) k'_i is negative and its two adjacent k'_{i-1} and k'_{i+1} are also negative, otherwise k_i should be cancelled as the singularity included, as shown in Figure 7.

The proposed FDD can be realized by adding the FDD part (in the dashed line) into the PA (power amplifier), as shown in Figure 8. As the same as in Figure 1, the upper part include a current control loop, and will provide electromagnetic coil with the load current equalling to the desired current i^*. The inputs of proposed FDD are the current sampling points from the current sensor, and these points will be restored in the queue, used to calculate the slope, as in Equation (19). A $\bar{k}$ calculating module is designed to cancel the singularities (if exist) and get the $\bar{k}$ value. The flow chart of the algorithm is shown in Figure 9. Theoretically, the $\bar{k}$ should be within the thresholds in Equation (9), or a fault of the electromagnetic actuator will be reported to upper controller. However, an adjustment can improve the accuracy of FDD, the detailed adjustment is discussed in the next Section 4.1.

4. Experimental results and analysis

The Experimental platform was built based on DSP (digital signal processor) TMS320F28335, as shown in Figure 10. We developed the controller and power circuit board, and employed the excitation signal generator, DS1302, controllable DC supply, and oscilloscope with 1 G samples/s.

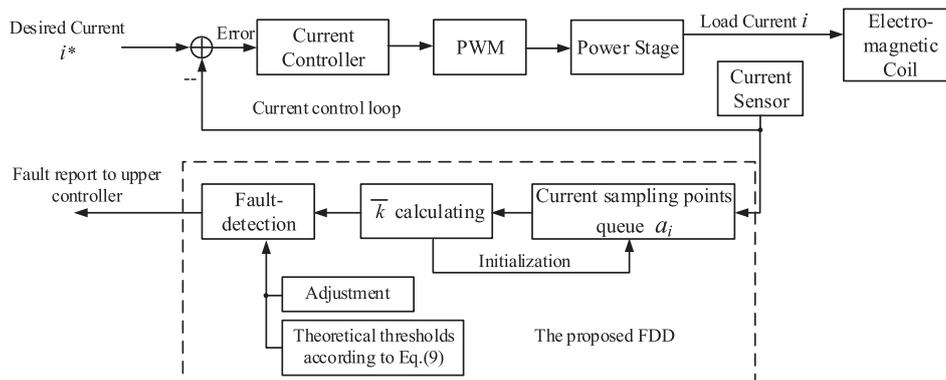Considering the sampling rate should be high enough, the switching period was set as 40 us @ 25 kHz,

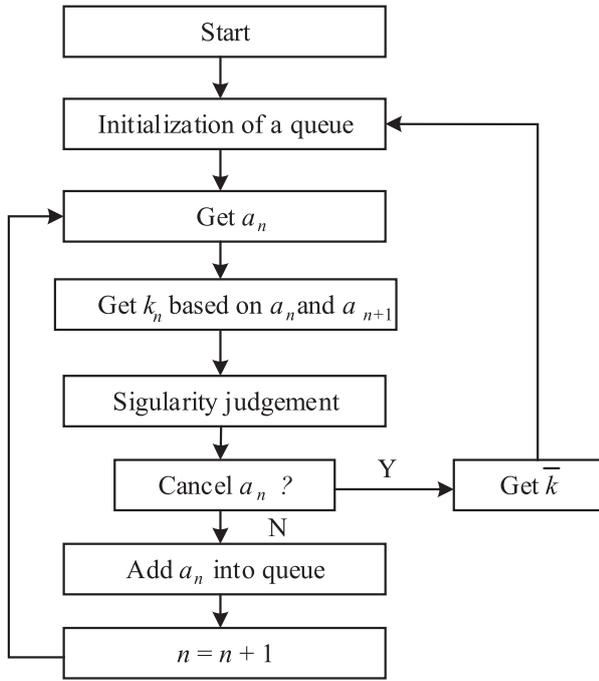**Figure 8.** Block diagram of proposed FDD.

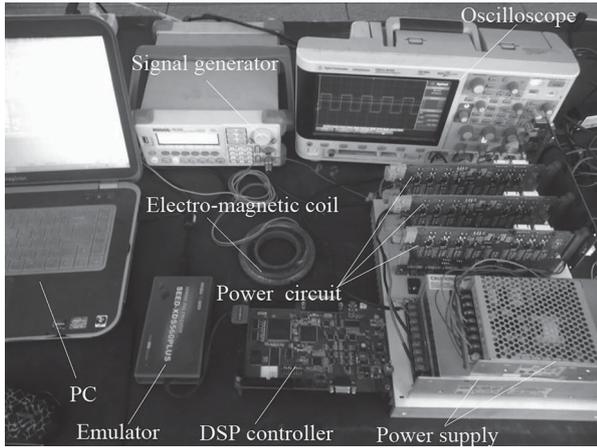**Figure 9.** Algorithm flow chart of $\bar{k}$ calculating.

Figure 10. Experimental platform.

while the sampling rate of current was 2.22 ms @ 450 kHz, therefore we can have 18 points sampled to calculate an equivalent slope $\bar{k}$ in the modulation. the operation cycle of the algorithm in DSP was about 1.75 ms.

In the experiment, we selected different electro magnetic coils to test the fault-diagnosis performance under different load condition, especially the variation characteristics under the change of the load. The initial coil was 1.75 mH, 0.5 Ω, corresponding to the time constant of 3.5 ms, which was much larger than the switching period of 40 us, proving the assumption in Section 2. In addition, the bus voltage U_d was 30 V, i_0 was 0.5 A and T was 40 us, so the theoretical range of slope of the load current is 16,761–16,857 A/s, according to Equation (9).
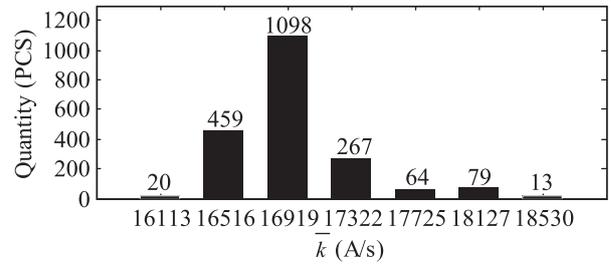

Figure 11. The histogram of $\bar{k}$ in a continuous 2000 sampling statistics.

4.1. Error analysis

There are some factors to influence the identification accuracy of equivalent slope, and the main error sources are as follows: (1) the drift and noise of the analogue signals, and the gain error of circuit. The total error caused was about 20 mV, corresponding to about 12 A/s error of equivalent slope. (2) Considering the electromagnetic coil as an energy storage element, a bus pumping will lead to bus voltage fluctuation, which is related to the configuration of power circuit. The measured peak was about 1 V, and the corresponding error (Δk) was about 570 A/s. (3) The variation of the air gap between the rotor and the magnetic pole will make influences to the equivalent inductance of the coil. Although the basis of the proposed approach is how to identify the time constant of electromagnetic coil, but not the model of actuator, we must still consider that the equivalent inductance of the coil will change under the variation of the air gap length $g(x, y)_j$. We can find the relationship between the air gap length and equivalent inductance of the electromagnetic coil in the following equation:

$$L_i = \frac{\mu_0 A N^2}{2(g_0 \pm \Delta)} \tag{21}$$

where g_0 and Δ are the initial air gap length and the variation, respectively. μ_0, A and N are the vacuum magnetic permeability, the area of magnetic pole and the number of the coil windings, respectively. Usually, we design auxiliary bearings to avoid the collision and friction between rotor and stator even when electromagnetic actuators fail, which will maintain air gap within a fixed range after the bearing structures designed. The maximum change of inductance value is 0.011 mH in the experiment, and the corresponding Δk is about 120 A/s. In summary, the total error is about 700 A/s, and Figure 11 is the histogram of $\bar{k}$ in a continuous 2000 sampling statistics.

The error sources above influence the identification accuracy of equivalent slope and it is difficult to have an accurate error model, so the measurement results in healthy electromagnetic actuators are only the ways to help to verify the effect of adjustment, in order to improve the accuracy of fault-diagnosis, but
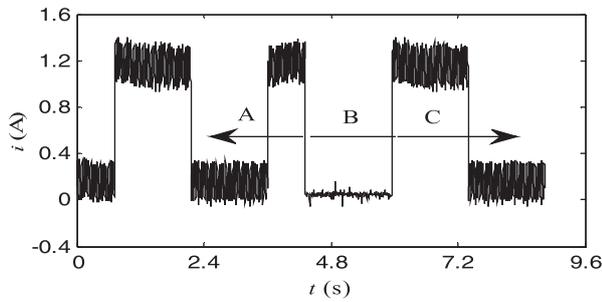
Figure 12. Broken circuit current waveform under pulse excitation signal at normal stage (A), fault stage (B), and fault-tolerant stage (C).

Figure 14. Range of slope, k'_{min} to k'_{max} correspond to normal stage, while the k_1 and k_2 correspond to broken circuit fault stage.

it does not mean that the theoretical thresholds were untrusted. Compared with theoretical thresholds of 16,761–16,857 A/s from Equation (9), the total adjustment was about 700 A/s only.

4.2. FDD of broken circuit

Figure 12 shows the current waveform measured in the experiment, which illustrates the normal stage, fault stage and fault-tolerant stage. Figure 13(a,b) plots the sampling points of load current at the normal stage (A) and fault stage (B), respectively, in which the obvious differences of current variation can be seen. Figure 14 illustrates the range of $\bar{k}$ from k'_{min} to k'_{max} at the normal stage, whose threshold values are determined by the theoretical values of Equation (9), and adjusted according to the actual statistics in Figure 11. k_1 and k_2 correspond to the maximum and minimum slope value under broken circuit condition, respectively, obviously those values are far away from the ones at the normal range.

Time for fault-diagnosis, t_d, is illustrated in Figure 15, in which the upper line is the fault-diagnosis flag, low-level for fault generated by the GPIO of DSP; lower line is the load current, obviously the t_d is about 2 ms for the broken circuit fault.

4.3. FDD of partial short circuit

In order to generate the partial short circuit of the electromagnetic coil, as in Figure 16, a switch was designed to change the load. Figure 17 shows the partial short-circuit current waveform measured in the experiment,
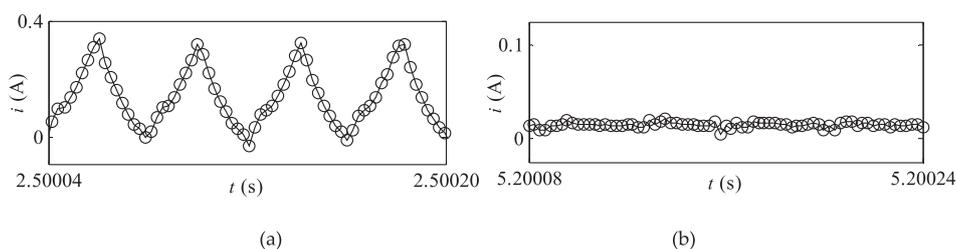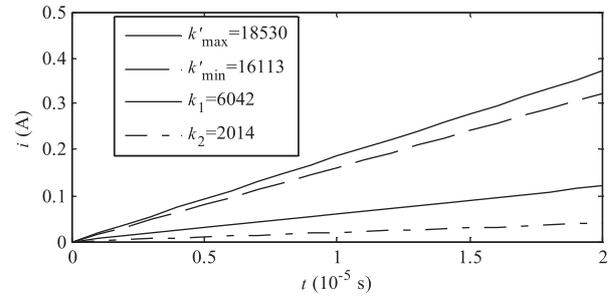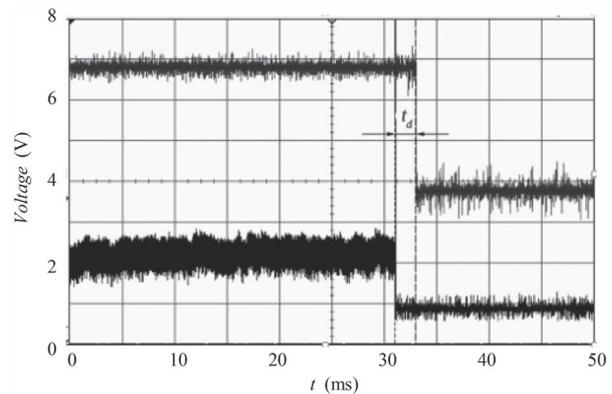

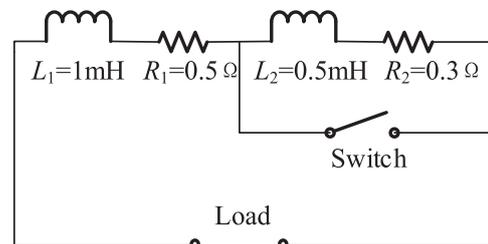**Figure 15.** Time for fault-diagnosis, t_d under broken circuit.

Figure 16. Load in experiment.

in which the range of the current ripple changes obviously. Figure 18 plots the sampling points of load current at normal stage and fault stage.

Figure 19 illustrates the k'_{min}, k'_{max}, k_1 and k_2 under partial short circuit, obviously there is a clearance between the ranges of normal stage and fault stage. Figure 20 illustrates the t_d of about 2 ms similarly.

(a)

(b)

Figure 13. Sampling points of load current at the normal stage (A) and the fault stage (B) under broken circuit.
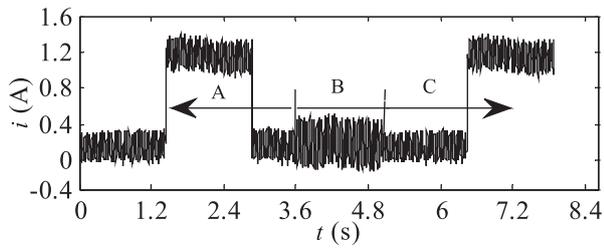
Figure 17. Partial short-circuit current waveform under pulse excitation signal at normal stage (A), fault stage (B), and fault-tolerant stage (C).
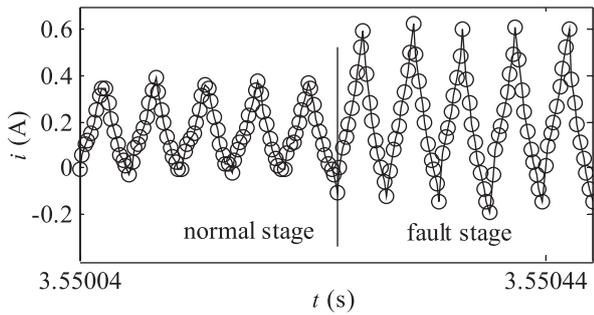

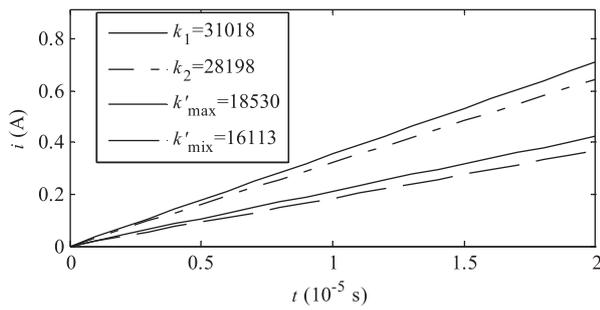**Figure 18.** Sampling points of load current at normal stage and fault stage under partial short circuit.

Figure 19. Range of slope, k'_{min} and k'_{max} correspond to normal stage, while the k_1 and k_2 correspond to partial short-circuit fault stage.
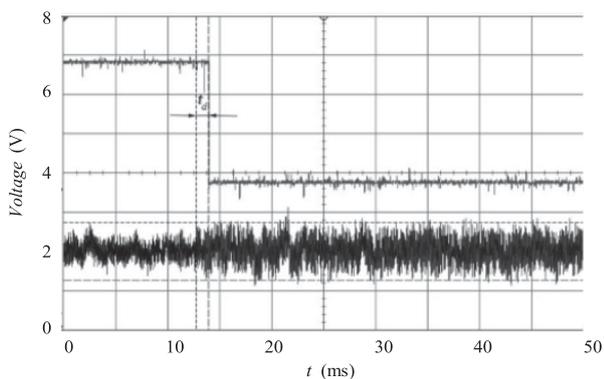

Figure 20. Time for fault-diagnosis, t_d under partial short circuit.

5. Conclusions

In this paper, an online fault-diagnosis approach of electromagnetic actuator is proposed, which is based on variation characteristics of load current in the switching period to identify the time constant of the electromagnetic coil. The experimental results demonstrate that:

(1) The proposed approach is effective to diagnose the broken circuit and partial short circuit of electromagnetic coil, and the fault-diagnosis time is about 2 ms for both faults.
(2) The variation characteristics of load current can be analysed in theory, the effectiveness of theoretical thresholds of range in normal stage has been proved. Equation (9) provides an effective way to get the theoretical thresholds. But what has to be admitted is that, some adjustments to theoretical thresholds will help to improve the accuracy of fault-diagnosis.

Future work should be focus on the follows:

(1) For both loosely and tightly coupled magnetic-levitated bearings, the proposed approach can provide a new idea for on-line fault-diagnosis of the electromagnetic actuators. Accurate and fast fault-diagnosis is the crucial foundation of fault-tolerance of magnetic-levitated bearings, and also the bottleneck of improving the real-time performance of the fault-tolerant controller. Therefore, a fault-tolerant controller with excellent real-time performance should be designed by combing the generalized bias current linearization in [37] with The proposed approach.
(2) Some adjustments to the theoretical thresholds can help to improve the accuracy of fault-diagnosis. However, we can only realize the adjustment calculation off-line in the different applications. The on-line adjustment calculation should be an interesting work in the future.

Disclosure statement

No potential conflict of interest was reported by the authors.

References

[1] Jansen JW, van Lierop CM, Lomonova EA, et al. Modeling of magnetically levitated planar actuators with moving magnets. IEEE Trans Magn. 2007;43(1):15–25.
[2] Okada Y, Nonami K. Research trends on magnetic bearings. Proceedings of the International Symposium on Magnetic Bearings; 2003. p. 341–342.

[3] Rovers JMM, Jansen JW, Compter JC, et al. Analysis method of the dynamic force and torque distribution in the magnet array of a commutated magnetically levitated planar actuator. IEEE Trans Ind Electron. 2012;59(5):2157–2166.

[4] Tu X, Zhou R, Zhou Y, et al. Dynamical decoupling and feed-forward control for magnetically levitated planar actuators. Int J Appl Electromagnet Mech. 2017;54(1):57–76.

[5] Tu X, Zhou R, Zhou Y, et al. Measurement of initial phase for movers in magnetically levitated planer actuators. Int J Appl Electromagnet Mech. 2015;49(1):91–104.

[6] Zhou R, Zhou Y, Liu G, et al. Analysis of the eddy force disturbance on foil-wound coils in magnetic levitated planar motion. Int J Appl Electromagnet Mech. 2014;46(1):299–312.

[7] Zhu Y, Zhang S, Mu H. Augmentation of propulsion based on coil array commutation for magnetically levitated stage. IEEE Trans Magn. 2012;48(1):31–37.

[8] Cheng X, Zhang L, Zhou R G, et al. Analysis of output precision characteristics of digital switching power amplifier in active magnetic bearing system. Automatika. 2017;58(2):205–215.

[9] Zhang C, Tseng KJ, Nguyen TD, et al. Stiffness analysis and levitation force control of active magnetic bearing for a partially-self-bearing flywheel system. Int J Appl Electromagnet Mech. 2011;36(3):229–242.

[10] Wang D. T, Miao Q KL. Prognostics and health management: a review of vibration based bearing and gear health indicators. IEEE Access. 2018;6:665–676.

[11] Wang D. T, L K. Theoretical investigation of the upper and lower bounds of a generalized dimensionless bearing health indicator. Mech Syst Signal Process. 2018;98:890–901.

[12] Borghesani P, Pennacchi P, Chatterton S. The relationship between kurtosis- and envelope-based indexes for the diagnostic of rolling element bearings. Mech Syst Signal Process. 2014;43:25–43.

[13] Liu T, Chen J, Dong G. Zero crossing and coupled hidden Markov model for a rolling bearing performance degradation assessment. J Vibrat Control. 2014;20(16):2487–2500.

[14] Yu J. Adaptive hidden Markov model-based online learning framework for bearing faulty detection and performance degradation monitoring. Mech Syst Signal Process. 2017;83:149–162.

[15] Lei Y, Li N, Lin J. A new method based on stochastic process models for machine remaining useful life prediction. IEEE Trans Instrum Meas. 2016;65(12):2671–2684.

[16] Keogh P, Cole MOT. Dynamics and control issues for fault tolerance. In: Schweitzer G, Maslen EH, editors. Magnetic bearings. Springer; 2009. p. 407–433.

[17] Cheng X, Wang B, Chen Q, et al. A unified design and the current ripple characteristic analysis of digital switching power amplifier in active magnetic-levitated bearings. Int J Appl Electromagnet Mech. 2017;55(3):391–407.

[18] Chilengue Z, Dente J, Branco P. An artificial immune system approach for fault detection in the stator and rotor circuits of induction machines. Electr Power Syst Res. 2011;81:158–169.

[19] Zhou W, Lu B, Habetler TG, et al. Incipient bearing fault detection via motor current noise cancellation using wiener filter. IEEE Trans Ind Appl. 2009;45:1309–1316.

[20] Li B, Zhang P-l, Wang Z-J, et al. A weighted multiscale morphological gradient filter for rolling element bearing fault detection. ISA Trans. 2011;50:599–608.

[21] Saidi L, Fnaiech F, Henao H, et al. Diagnosis of broken-bars fault in induction machines using higher order spectral analysis. ISA Trans. 2013;52:140–148.

[22] Bouzida A, Touhami O, Ibtiouen R, et al. Fault diagnosis in industrial induction machines through discrete wavelet transform. IEEE Trans Ind Electron. 2011;58:4385–4395.

[23] Gu F, Wang T, Alwodai A. A new method of accurate broken rotor bar diagnosis based on modulation signal bispectrum analysis of motor current signals. Mech Syst Signal Process. 2015;50–51:400–413.

[24] Cade IS, Keogh PS, Sahinkaya MN. Fault identification in rotor/magnetic bearing systems using discrete time wavelet coefficients. IEEE/ASME Trans Mechatron. 2005;10(6):648–657.

[25] Nagel L, Galeazzi R, Voigt AJ, et al. Fault diagnosis of active magnetic bearings based on Gaussian GLRT detector. Control and Fault-Tolerant Systems; IEEE; 2016. p. 540–547.

[26] Panadero RP, Sanchez MP, Guasp MR, et al. Improved resolution of the MCSA method via Hilbert transform, enabling the diagnosis of rotor asymmetries at very low slip. IEEE Trans Energy Convers. 2009;24:52–59.

[27] Noel NK, Tammi K, Buckner GD, et al. Intelligent Kalman filtering for fault detection on an active magnetic bearing system. IEEE Trans Comput Aided Des Integr Circuits Syst. 2008;25(12):2757–2764.

[28] Tsai NC, King YH, Lee RM. Fault diagnosis for magnetic bearing systems. Mech Syst Signal Process. 2009;23(4):1339–1351.

[29] Aydin I, Karakose M, Akin E. An approach for automated fault diagnosis based on a fuzzy decision tree and boundary analysis of a reconstructed phase space. ISA Trans. 2014;53:220–229.

[30] Nguyen NP, Hong SK. Sliding mode thau observer for actuator fault diagnosis of quadcopter UAVs. Appl Sci. 2018;8:1893.

[31] Nguyen NP, Hong SK. Fault diagnosis and fault-tolerant control scheme for quadcopter UAVs with a total loss of actuator. Energies. 2019;12:1139.

[32] Glowacz A. Recognition of acoustic signals of commutator motors. Appl Sci. 2018;8:2630.

[33] Freddi A, Longhi S, Monteriù A. A diagnostic thau observer for a class of unmanned vehicles. J Intell Robot Syst. 2012;67:61–73.

[34] Shahnazari H, Mhaskar P. Actuator and sensor fault detection and isolation for nonlinear systems subject to uncertainty. Int J Robust Nonlin Control. 2017;28(6):1996–2013.

[35] Florian L. Detection and correction of actuator and sensor faults in active magnetic bearing system. 8th International Symposium on Magnetic Bearing; 2002 Aug 26–28; Mito, Japan.

[36] Zhao K, Li P, et al. Sliding mode observer-based current sensor fault reconstruction and unknown load disturbance estimation for PMSM driven system. Sensors. 2017;17:2833.

[37] Maslen E H, Meeker D C. Fault tolerance of magnetic bearings by generalized bias current linearization. IEEE Trans Magn. 1995;31(3):2304–2314.

[38] Cheng X, Liu H, Song S, et al. Reconfiguration of tightly-coupled redundant supporting structure in active magnetic bearings under the failures of

electro-magnetic actuators. Int J Appl Electromagnet Mech. 2017;54:421–432.

[39] Noh MD, Cho S-R, Kyung J-H, et al. Design and implementation of a fault-tolerant magnetic bearing system for turbo-molecular vacuum pump. IEEE/ASME Trans Mechatron. 2005;10(6):626–631.

[40] Cheng X, Chen Q, Zeng H, et al. Reconfiguration rules for loosely-coupled redundant supporting structure in radial magnetic bearings. Int J Appl Electromagnet Mech. 2016;51(2):91–106.

[41] Na UJ, Palazzolo A. Optimized realization of fault-tolerant heteropolar magnetic bearings. Trans ASME J Vib Acoust. 2000;122(3):209–221.

[42] Li M-H, Palazzolo A, Kennyetal A. Fault-tolerant homopolar magnetic bearings. IEEE Trans Magn. 2004;40(5):3308–3318.